

1 Upper Ocean Response on the Passage of Tropical Cyclones in 2 the Azores Region

3 Miguel M. Lima¹-(malima@fe.ul.pt), Célia M. Gouveia^{1,2}-(cmgouveia@fe.ul.pt), Ricardo M.
4 Trigo^{1,3}-(rmtrigo@fe.ul.pt)

5 *Correspondence to:* Miguel M. Lima-(malima@fe.ul.pt)

6 ¹Instituto Dom Luiz (IDL), Faculdade de Ciências, Universidade de Lisboa, 1749-016, Lisboa, Portugal

7 ²Instituto Português do Mar e da Atmosfera (IPMA), I.P., 1749-077, Rua C do Aeroporto, Lisboa, Portugal

8 ³Departamento de Meteorologia, Universidade Federal do Rio de Janeiro, Rio de Janeiro 21941-919, Brasil

9 **Abstract.** Tropical Cyclones (TCs) are extreme climate events that are known to strongly interact with the ocean
10 through two mechanisms: dynamically through the associated intense wind stress, and thermodynamically through
11 moist enthalpy exchanges at the ocean surface. These interactions contribute to relevant oceanic responses during and
12 after the passage of a TC, namely the induction of a cold wake and the production of chlorophyll (~~chl~~Chl-a) blooms.
13 This study aimed to understand these interactions in the Azores region, an area with relatively low cyclonic activity
14 for the North Atlantic basin, since the area experiences much less intense events than the rest of the basin. Results for
15 the 1998-2020 period showed that the averaged induced anomalies were on the order of $+0.026050 \text{ mg/m}^3 \text{ m}^{-3}$ for the
16 ~~chl~~Chl-a and -1.554615 K for SST. Furthermore, looking at the role played by several TCs characteristics we found
17 that the intensity of the TCs was the most important condition for the development of upper ocean responses. ~~Two~~
18 ~~other analysed conditions were the TC's translation speeds and the impacted areas, which also showed to be positively~~
19 ~~affecting the registered induced anomalies.~~ Additionally, it was found that bigger TCs induced greater anomalies in
20 both variables, while faster ones created greater Chl-a responses, and TCs that occurred later in the season had greater
21 anomalies. Two case studies (Ophelia, in 2017, and Nadine, in 2012) were conducted to better understand each upper
22 ocean response. Ophelia showed to affect the SST at an earlier stage while the biggest ~~chl~~Chl-a induced anomalies
23 were registered at a later stage, allowing the conclusion that thermodynamic exchanges conditioned the SST more
24 while dynamical mixing might have played a more important role in the later stage. Nadine showed the importance of
25 the TC track geometry, revealing that the TC track observed in each event can impact a specific region for longer, and
26 therefore induce greater anomalies.

27 Introduction

28 Tropical Cyclones (TCs) are potentially intense atmospheric disturbances which are characterised by a low-pressure
29 centre (eye) where strong winds curl around. Among other important properties, TCs are thermodynamic dependent
30 phenomena, meaning that intense temperature gradients need to occur in the lower atmosphere to maintain and
31 intensify the storm. Thus, TCs are fed from warm sea water which provide a strong moist enthalpy flux from the

32 oceanic surface to maintain a steep temperature gradient within the lower and middle troposphere and produce massive
33 water vapour convection (Emanuel, 2003; Holton ~~&~~and Hakim, 2012; Pearce, 1987).

34 The strong wind stress present near the surface and the associated intense curl are also shown to induce vertical mixing
35 and Ekman upwelling in the upper layer of the ocean. In ~~the~~his seminal study-by₂, Price (1981) ~~it is shown~~shows,
36 through both observed and numerical modelling data, the evolution of sea surface temperature (SST) on the passage
37 of a hurricane, with the emergence of a cold wake of SST after a TC due to entrainment of water from shallow layers.
38 This effect has since been well studied and documented with many case studies observed, for example, the case of
39 Hurricane Felix, in the vicinity of Bermuda in 1995, that showed decreases in the order of 3.5-4 °C (Dickey *et al.*,
40 1998), or the cases of cyclones Nargis (2008) and Laila (2010), in the Bay of Bengal, that caused SSTs to drop by
41 around 1.76 °C (Manceesha *et al.*, 2012). Additionally, several model-based works ~~have been done~~focused on either
42 ~~according to the~~ ~~effect~~effects caused by the TCs, ~~as well as~~or the interaction of the TC with its own cold wake (e.g.,
43 Chen *et al.*, 2017; Zhang *et al.*, 2019).

44 There are also biological responses to the passage of a TC. Due to the upwelling of colder water, ~~there may also occur~~
45 ~~the~~transport of nutrient-rich water from the sub-superficial layer ~~may also occur~~ (Kawai ~~&~~and Wada, 2011). In this
46 case, phytoplankton can quickly increase in the surface layer following the rise in nutrients. This increase can be
47 remotely sensed through satellite observations that capture the chlorophyll-a concentration (Chl-a) increasing after the
48 passage of a TC, since ~~chl~~Chl-a is generally accepted as a proxy for biological activity (Kawai ~~&~~and Wada, 2011; Liu
49 *et al.*, 2009; Subrahmanyam *et al.*, 2002; Walker *et al.*, 2005).

50 The oceanic response, either physical or biological, to the passage of a TC depends on various aspects, most
51 remarkably the TC's intensity and its translation speed but also the oceanic subsurface conditions (Zheng *et al.*, 2008).
52 The magnitude and significance of these aspects on the modulation of the oceanic response varies regionally, although
53 it is generally regarded that the most impactful phenomena to be those of an intense and slow TC (Chacko, 2019;
54 Price, 1981; Price *et al.*, 1994). Recent studies (e.g., Chacko, 2019; Pan *et al.*, 2018; Shropshire *et al.*, 2016) have
55 shown that regional differences do matter when studying the biological response. In the case of the Bay of Bengal, it
56 was shown that the intensity of a TC is less important, and the most meaningful aspects are the TC's translation speed
57 and, to a lesser degree, a pre-existing shallow mixed layer (Chacko 2019). The results from this study are important
58 to stress that relatively weaker TCs can also induce a strong biological response after their passage.

59 Until now, the Azores region has not been studied regarding its thermodynamic and biological impacts. This section
60 of the North Atlantic basin presents much fewer and weaker cyclones than the tropical band of the basin, with this
61 region being mainly a zone where TCs undergo either cyclosis or post-tropical transition into extra-tropical cyclones
62 or mid-latitude storms (Baatsen *et al.*, 2015; Haarsma *et al.*, 2013). The north-eastern Atlantic (NEA) basin, where the
63 Azores archipelago is located, presents significantly less TCs than the western counterpart, closer to the USA coast
64 (Baatsen *et al.*, 2015; Lima *et al.*, 2021; Haarsma *et al.*, 2013). However, there is growing evidence of a significant
65 increase in the frequency of strong TCs in both western (Kossin *et al.*, 2020) and eastern (Lima *et al.*, 2021) halves of
66 the north Atlantic Ocean. The climatology of the area points to a south-north gradient in both SST and ~~chl~~Chl-a, with

67 a decrease in the former and an increase in the latter (Amorim et al., 2017); [Caldeira and Reis, 2017](#)). In general, the
68 southern part of the Azores region offers SSTs high enough to maintain TCs, although the necessary atmospheric
69 conditions (e.g., high lapse rates and low wind shear) need to occur for their passage northeast through the Azores
70 (Lima et al., 2021). However, this area is undergoing a transition due to anthropogenic climate change and an increase
71 both in number and intensity of TCs is expected (Baatsen et al., 2015; Haarsma et al., 2013). Therefore, the NEA basin
72 is a challenging study region to assess the impact that lower intensity TCs have on the oceanic surface.

73 The main aim of this study is to analyse in detail the upper ocean response observed after the passage of a TC in the
74 Azores region, which is characterised by its lower-than-normal cyclonic activity in relation to the rest of the north
75 Atlantic basin. In particular, we aim to evaluate the impacts on ~~sea surface temperature (SST)~~ and ~~ehlorophyll~~[Chl-a](#)
76 concentration (~~Chl-a~~) produced by ~~three~~ important TC characteristics (averaged maximum wind speed, ~~emulative~~
77 ~~impacted area, and~~ average translation speed, ~~overall impacted area, time of occurrence, and geometry of the track~~).
78 Two practical case studies, relative to Nadine (2012) and Ophelia (2017) are then thoroughly analysed to reflect the
79 drawn conclusions for this area.

80 **Data**

81 ~~Data~~[The main data](#) used to evaluate the oceanic response in this study is divided into three main parts: Remotely
82 sensed [interpolated](#) data used to characterise the ~~eh~~[Chl-a](#) and SST, respectively, and TC track data, which provides
83 the necessary additional information on the location and dynamic variables of each TC, that allow to explore the
84 oceanic response in the aforementioned data. [Additionally, non-interpolated datasets are used for the case studies to](#)
85 [validate the interpolated ones; and wind-stress data is used for the Hurricane Ophelia study case.](#)

86 Biological oceanic response was evaluated using a multi-sensor daily ~~eh~~[Chl-a](#) product available through the
87 Copernicus Marine Environment Monitoring Service (CMEMS) in a 4 km x 4 km resolution from the end of 1997 to
88 the present (CMEMS, 2021b). This product, delivered by the ACRI-ST company, is based on the Copernicus-
89 GlobColour project and obtained by merging different sensors: SeaWiFS, MODIS, MERIS, VIIRS-SNPP&JPSS1,
90 OLCI-S3A&S3B. The final ~~eh~~[Chl-a](#) product is a mix of several algorithms that consider different water conditions,
91 such as oligotrophic, mesotrophic, coastal, clear, and complex waters (Garnesson et al., 2019). To produce a “cloud
92 free” product, the resulting data was subjected to daily interpolation to fill any gaps (Krasnopolsky et al., 2016;
93 Saulquin et al., 2019). The lack of gaps in this dataset is particularly relevant in the context of this study since the
94 areas analysed will be concentrated around the TCs; it is then expected that large amounts of the analysed areas would
95 be under cloud coverage and, therefore, some of the analysed data is not real but interpolated values. [Nonetheless,](#)
96 [CMEMS provides approximate uncertainty levels for this data, which we used to assess the quality of our results. For](#)
97 [further validation purposes we used also a non-interpolated Chl-a product generated by the Ocean Colour component](#)
98 [of the European Space Agency’s Climate Change Initiative project \(OC-CCI\) \(Sathyendranath et al., 2019\). This](#)
99 [dataset results from a merge of several sensors: SeaWiFS LAC and GAC, MODIS Aqua, MERIS, VIIRS, and OLCI.](#)

100 [ESA's OCC-CI version 5.0 Chl-a product has 0.042° resolution and a daily temporal resolution \(Sathyendranath et al.,](#)
101 [2021\).](#)

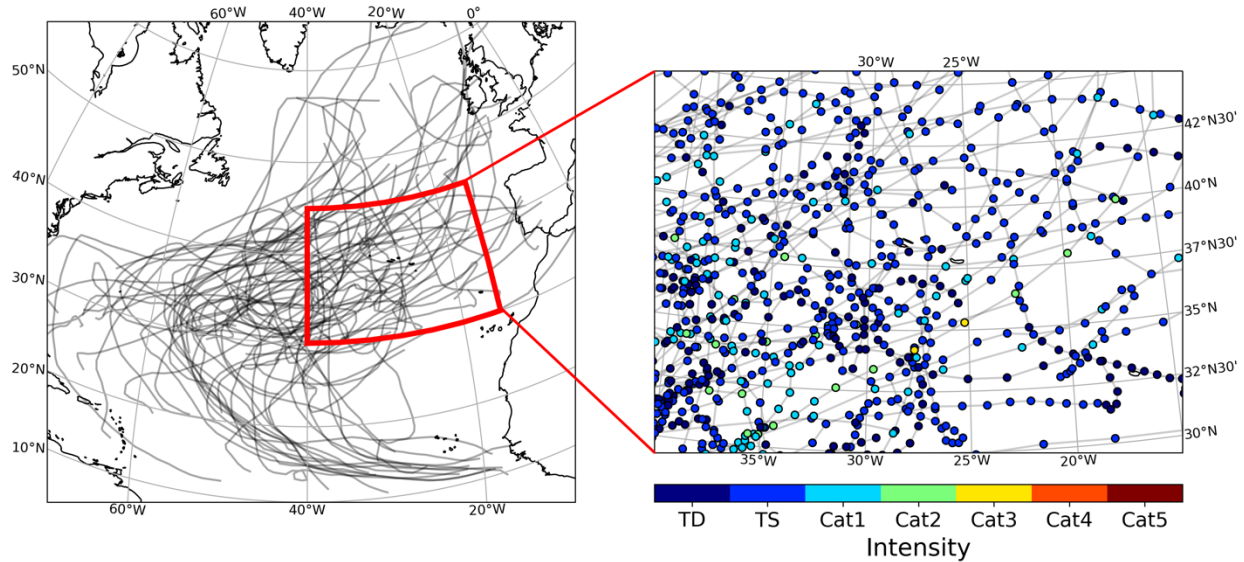
102 To evaluate the physical oceanic response and to relate this to the biological one, a daily SST dataset from the CMEMS
103 was used, with a 0.05° resolution. This data is available from 1981 up to the near present (CMEMS, 2021a). Similarly,
104 to the previous ~~cm~~[CMEMS interpolated Chl-a](#) product the SST field is also a blended gap-free analysis product, with
105 the present one resulting from re-processed (A)ATSR, SLSTR and AVHRR sensor data being applied to the
106 Operational SST and Sea Ice Analysis (OSTIA) system (Donlon et al., 2012). This reprocessed analysis product
107 provides an estimate of the SST at 20 cm depth. The inputs to the system are SSTs at 10:30 am and 10.30 pm local
108 time which means that the analyses roughly correspond to the daily average SST (Good et al., 2020; Lavergne et al.,
109 2019; Merchant et al., 2013). [As stated before, approximated error values for SST are also provided by CMEMS.](#)
110 [Additionally, AVHRR Pathfinder version 5.3 collated data was used as non-interpolated data for validation. This](#)
111 [dataset, similarly to the CMEMS one, is a collection of twice-daily \(averaged to daily\), 4km spatial resolution, merged](#)
112 [SST product, provided by NOAA's National Centers for Environmental Information \(Saha et al., 2018\). The merge](#)
113 [of this data, however, is only used to spatially collate the data, as it is a single instrument measurement \(AVHRR\)](#)
114 [onboard NOAA-7 through NOAA-19 Polar Operational Environmental Satellites \(POES\).](#)

115 [Wind stress data to assist in the analysis of the Hurricane Ophelia study case was provided by NOAA's CoastWatch](#)
116 [dataset available at \[https://coastwatch.pfeg.noaa.gov/erddap/griddap/erdQMstress1day_LonPM180.html\]\(https://coastwatch.pfeg.noaa.gov/erddap/griddap/erdQMstress1day_LonPM180.html\). This dataset](#)
117 [is derived from wind measurements obtained from the Advanced Scatterometer \(ASCAT\) instrument on board](#)
118 [EUMETSAT's MetOp satellites \(A and B\) at a daily 0.25° resolution, from 2013 to the present. ASCAT presents a](#)
119 [near all-weather capacity \(not affected by clouds\), as it operates a frequency in C-band \(5.255 GHz\), therefore,](#)
120 [minimizing the number of missing values in predominately clouded areas such as the case of TC paths.](#)

121 The TC track data is made available by the *International Best Track Archive for Climate Stewardship Project* version
122 4 (IBTrACS v4) free access dataset (Knapp *et al.*, 2009). This dataset contains global information regarding TC
123 activity since the 1851 hurricane season up to ~~the most recent full hurricane season, 2020-2020~~. It aggregates variables
124 such as TC geographical location, maximum wind speed, minimum sea level pressure, and storm radius estimation
125 based on wind intensity, measured at 6-hour intervals (original dataset interpolates for increased resolution, at 3-hour
126 rates, however this interpolation only includes the geographical location). For the 1998-2020 period, the Azores
127 region experienced the passage of 62 individual TCs accounting to 642 6-hour observations that are categorised in the
128 following intensities according to the Saffir-Simpson hurricane wind scale (Taylor *et al.*, 2010):

- 129 ● 148 tropical depression observations.
- 130 ● 389 tropical storm observations.
- 131 ● 85 category 1 hurricane observations.
- 132 ● 18 category 2 hurricane observations.
- 133 ● 2 category 3 hurricane observations.

134 The full TC tracks can be better visualised in Fig. 1, with the left panel showing the full track for all these 62 TCs'
135 observed in the NA basin for the 1998-2020 period and the right panel showsshowing a zoomed view relative to the
136 considered Azores region. Tropical depression observations (dark blue in Fig. 1, right panel) account for 23 % of the
137 total observations and will not be considered in this study, as they present the lower branch of intensities with winds
138 below the 34-kt (18 m/s) threshold. Therefore, a total of 494 TC 6-hour observations were considered for this study.



139
140 **Figure 1 - Left panel: North Atlantic basin and the tracks for all TCs that went through or occurred inside the study region**
141 **(shown by the red outline). Right panel: Zoom of the previous red outline, with each TC observation marked in different**
142 **colours for intensity (TD: Tropical Depression; TS: Tropical Storm; Cat1 - Cat5: Hurricane category according to the**
143 **hurricane Saffir-Simpson wind scale).**

144 Since the interpolated datasets used for most of this study do not share the same time frame and to better encapsulate
145 full years of data, the timeframe of the present study will be from January 1st of 1998 to December 31st of 2020.
146 Moreover, while we have extracted all the data described above covering the entire North Atlantic basin, we will focus
147 on the area around the Azores archipelago, delimited by the 15°W and 40°W meridians and between the 30°N and the
148 45° parallels- (Fig. 1).

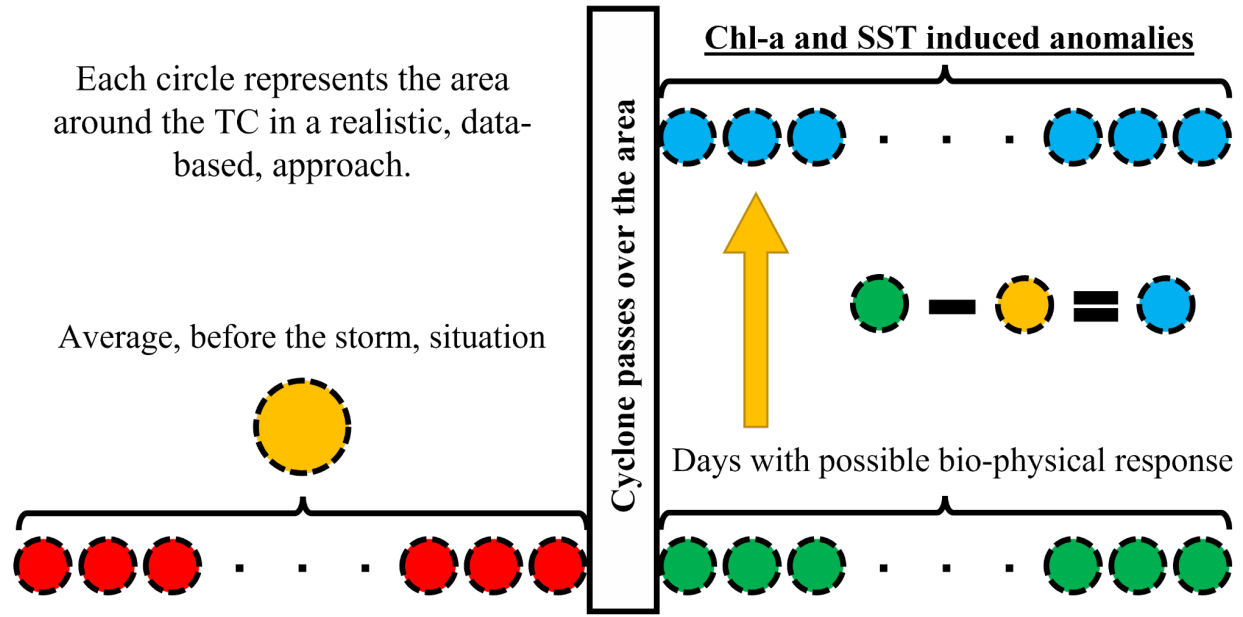
149 Methodology

150 The area of focus on this study is centred in the Azores archipelago in the North Atlantic basin, pictured in Fig. 1. The
151 area is longitudinally delimited by the 15°W and 40°W meridians and latitudinally between the 30°N and the 45°
152 parallels. This region of study was chosen due to its nature regarding TCs, since it is an area with fewer and less
153 quantity and intensity of intense tropical storms (Hart & Evans, 2001; Lima et al., 2021; Ramsay, 2017). Generally,
154 tropical cyclosis and post-tropical transition occurs occur here (Baatsen et al., 2015; Haarsma et al., 2013). Because of
155 these aspects, it corresponds to a much less studied area and is a good region to characterise oceanic bio-

156 ~~physical~~biophysical effects after the passage of (generally) weaker TCs at higher-than-tropical latitudes, and to
157 compare the obtained results with previous literature.

158 To cope with large amounts of data, the bio-physical response was evaluated within a small area around individual
159 locations obtained for each TCs' best-track location. For this, we used the approximated quadrant radius given by the
160 IBTrACS v4 dataset. This dataset provides different types of radii depending on the considered isotach, for this study
161 we used the 34-kt isotach as it corresponds to the lower-bound for the Tropical Storm status according to the Saffir-
162 Simpson hurricane wind scale (Taylor et al., 2010). Since the considered area of analysis ~~would be falls~~
163 kt isotach, ~~any~~ tropical ~~depression observation was~~depressions were not considered (exact partition of intensities is
164 given at the beginning of the *Results* section). ~~To correct~~There are some missing radii values in the middle of TC
165 tracks, ~~and in order to correct~~ a simple linear regression was applied. ~~An example~~To illustrate the application of this
166 methodology ~~can be observed~~we present the study cases in Figs. 6a~~the results and 7a~~discussion section, for hurricanes
167 Ophelia (2017) and Nadine (2012), ~~respectively.~~. From inside this area of analysis, we may retrieve the ~~chl~~Chl-a
168 concentration and SST at their respective resolution, ~~as well as study their anomalies and post-storm responses.~~. The
169 analysis inside the considered area ~~is made recurring to~~was performed using histograms, in which each pixel inside
170 the 34-kt isotach contributes to that ~~TC's observation~~TCs histogram.

171 ~~To analyse the TCs' impact on their passage, a different approach was taken than the typical anomaly analysis since~~
172 ~~the effects caused by a TC may not be visible in simple anomalies computed against climatology. Some authors~~
173 ~~suggest that an appropriate time window to analyse the maximum bio physical oceanic response would be~~
174 ~~approximately circa 10 days after the passage of a TC (Kawai & Wada, 2011). To assess the best temporal window~~
175 ~~for our region, we analysed the daily anomalies registered between 30 days before and 30 days after the passage of a~~
176 ~~TC. Afterwards, we chose two time windows to reflect different situations (Fig. 2): (a) An average, before the storm,~~
177 ~~situation, which is required to assess the oceanic conditions before the TC occurred in the area (i.e., average of red~~
178 ~~circles in Fig. 2, resulting in yellow circle); (b) And secondly, a time window after the TC passed over the area,~~
179 ~~impinging the most significant response (Green circles, Fig. 2). Based on these definitions the induced anomaly can~~
180 ~~be calculated (blue circles, Fig. 2) by subtracting each daily value of (b) from the average situation before the storm~~
181 ~~described in (a). In the end, this leaves us with a large pool of observed daily induced anomalies to study, from which~~
182 ~~we may study the responses according to different TC intensities, translation speeds, or affected area.~~



183

184 **Figure 2—Resumed schematic of the applied methodology in each TC observation. Do note that the circles are a mere**
 185 **representation of each affected area. The colour coding follows: Red—Individual daily observations before the TC; Green**
 186 **—Individual daily observation after the TC passes over the region; Yellow—Averaged values before the TC; Blue—**
 187 **Individual daily induced anomalies. A more detailed description of the methodology is presented in the text.**

188 To analyse the TCs’ impact on their passage, inspiration was taken from Kawai and Wada (2011), who computed the
 189 climatic monthly standard deviation of Chl-a on 0.25° grids over a 5-year study period. Here, we computed for each
 190 storm the daily standard deviation of both Chl-a and SST over their respective grids relative to the climatology over
 191 the same area (only the area impacted by the TC was considered) for the study’s complete time frame; this analysis
 192 was performed considering 30 days before and after each TC to allow then the analysis of an ideal window to compute
 193 the induced anomalies. To compute this ideal window, we searched for the maximum difference between the number
 194 of standard deviations over the climatological value before and after the storm.

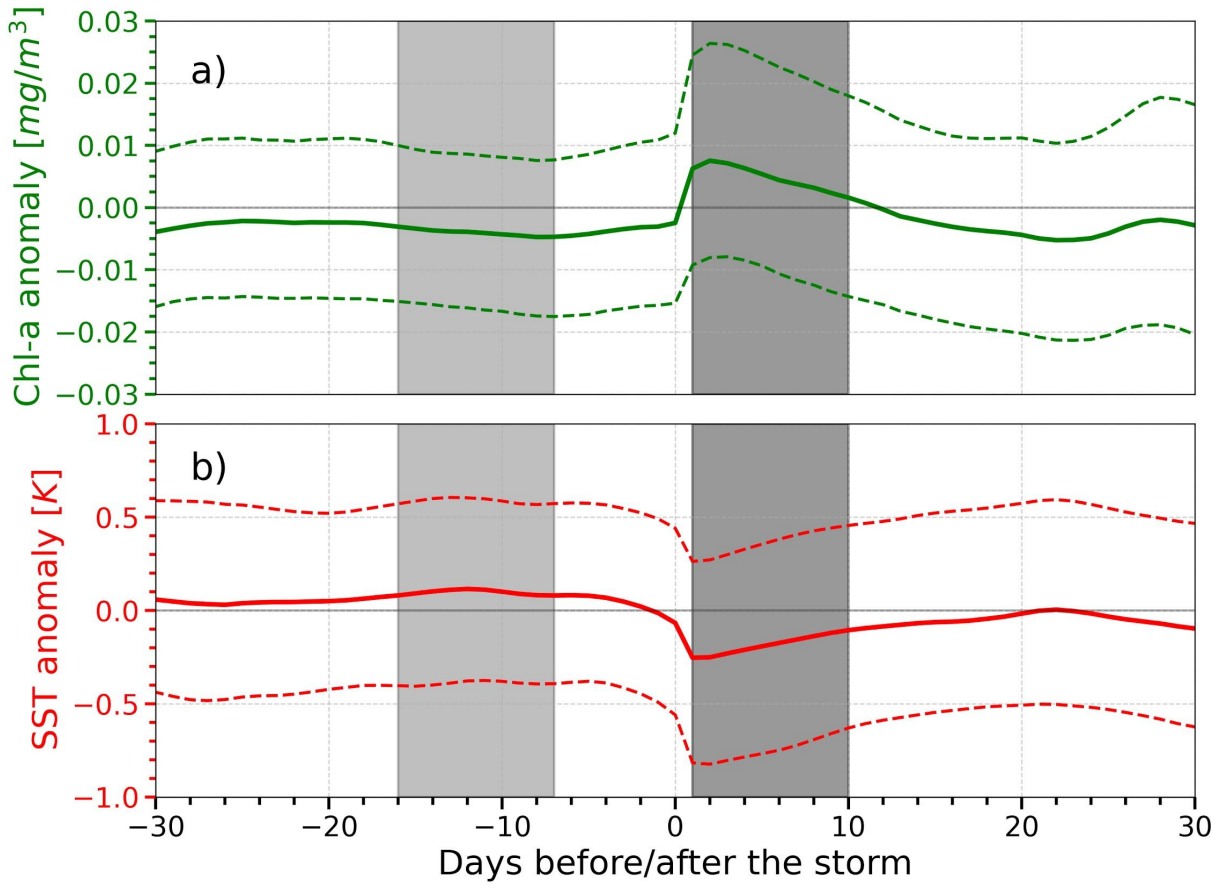
195 To compromise between having the maximum difference and ensuring a time window as close as possible to the storm
 196 (to minimize external factors to the TC), we performed a sensibility study on the length and location of the considered
 197 time window. First, we analyse the overall maximum difference in the 61-day period (including the day of the storm)
 198 and then search for a secondary maximum value that is within 10% of it considering a smaller sample of days,
 199 decreasing in groups of 5 days each time this search is made (e.g., the first iteration would be 25 days before and 30
 200 after, the second 30 before and 25 after, the third 25 before and after, etc.), until an optimum maximum difference
 201 value is identified. With this window defined, the induced anomalies are simply the difference between the daily
 202 values of Chl-a or SST after and before the TC.

203 As an example of this methodology, Fig. 2 shows the Chl-a standard deviation over the climatological value in the
 204 case of Hurricane Nadine. In this case, only 15 days around the TC are shown for clarity. We can see that the maximum
 205 difference is obtained between 8 days before and 1 day after the storm ($\Delta\text{Chl-a max}$). However, when we take into

206 account the compromise of considering windows located as close as possible to the occurrence of the TC over the
207 region, we see that the value found between 4 days before and 1 day after is within 10% of the absolute maximum.
208 This methodology is then applied to all 6-hour observations individually and for each TC, thus resulting in two groups
209 of induced anomalies (per TC and per 6-hour observations) where we can study these with respect to the TCs averaged
210 (per TC) or instantaneous (6-observations) characteristics.

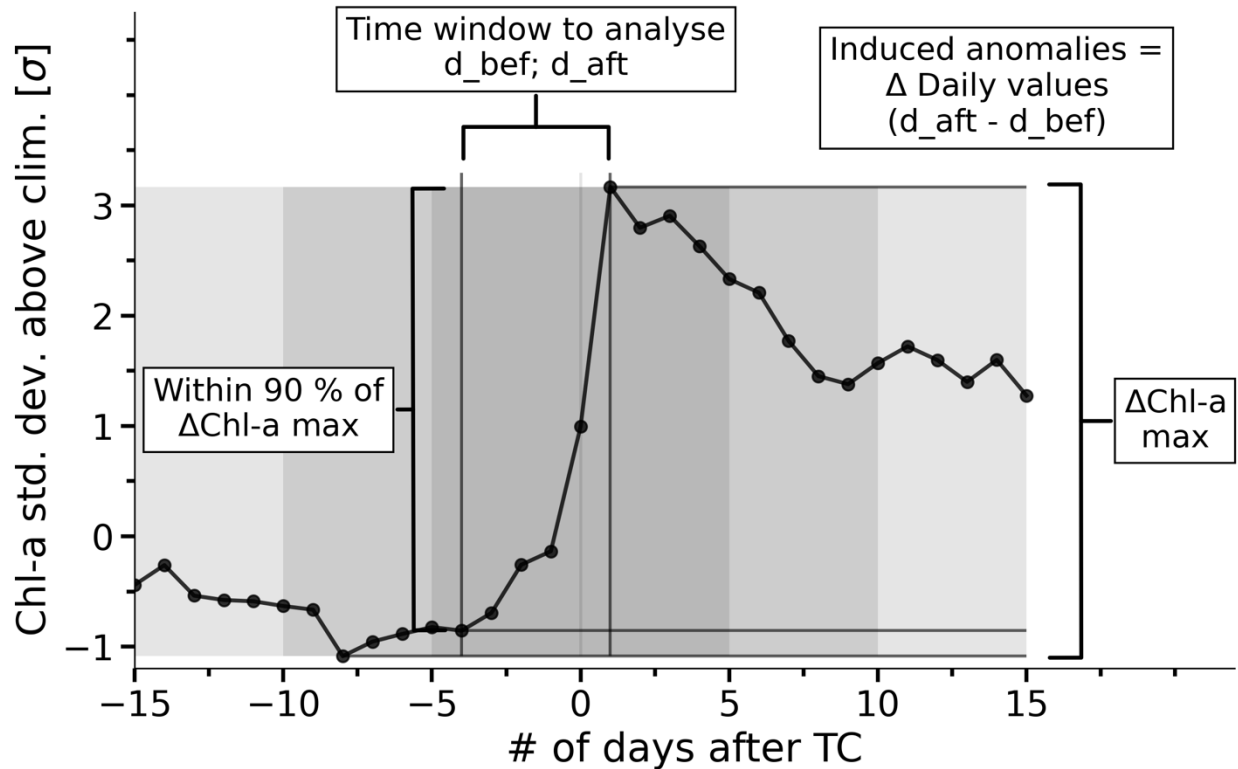
211 To address the possibility that some pixels are overlaid on top of each other, which would contaminate the analysis,
212 as observed in the case of the slow erratic Hurricane Nadine (~~track seen in Fig. 7~~presented in the *results and*
213 *discussion* section as a study case), we did not take into consideration the days in which the TC is over the
214 aforementioned overlaid region. ~~Therefore~~In these cases, the days considered are those ~~after~~when the ~~eye~~TC has
215 completely travelled over ~~these areas~~the area (i.e., that pixel is no longer inside the radius of influence of the TC).
216 However, when we consider independent 6-hour observations, this caveat cannot be accounted for since we have no
217 way of knowing if that area has been influenced or not by the TC before, for how long, or even if a future observation
218 will impact the area.

219 ~~To identify the appropriate time periods in this analysis we used a linear kernel change point detection algorithm that~~
220 ~~detects changes in the mean of any given signal (Celisse et al., 2018; Truong et al., 2020). Figure 3 shows the daily~~
221 ~~distribution of the Chl a (Fig. 3a) and SST (Fig. 3b) anomalies 30 days before and after the TC passed over a given~~
222 ~~area. Using the change point detection algorithm, we identified 2 main periods associated with this passage: i) 7 to 16~~
223 ~~days before the TC, representing an average condition prior to the arrival of the TC; ii) from 1 to 10 days after the~~
224 ~~period where it is clearly visible the effects on the oceanic variables. It is important to note that more periods were~~
225 ~~identified in between and after those presented due to the sensitivity of the algorithm but were not considered in the~~
226 ~~analysis for being too small or not showing relevance in our study (e.g.: from -17 to -30 days, or -4 to +1 days). The~~
227 ~~main 2 identified periods coincided in both cases (Figs. 3a and 3b), while those extra periods varied both in number~~
228 ~~and location.~~



229

230 **Figure 3** — Average daily a) chl-a (green solid line) and b) SST (red solid line) anomalies registered in a month period
 231 before/after each TC observation. Dotted lines show the first and third quartiles of each day. Shaded light grey area
 232 represents the period (-16 to -7 days) considered for the computation of the average before the storm situation and the
 233 darker grey represents the time period (+1 to +10 days) used to compute the induced anomalies.



234

235 [Figure 2 - Schematic of the applied methodology for each TC. Black line shows the number of standard deviations from the](#)
 236 [climatological values for the area surrounding Hurricane Nadine. A detailed description of this methodology can be found](#)
 237 [in the text.](#)

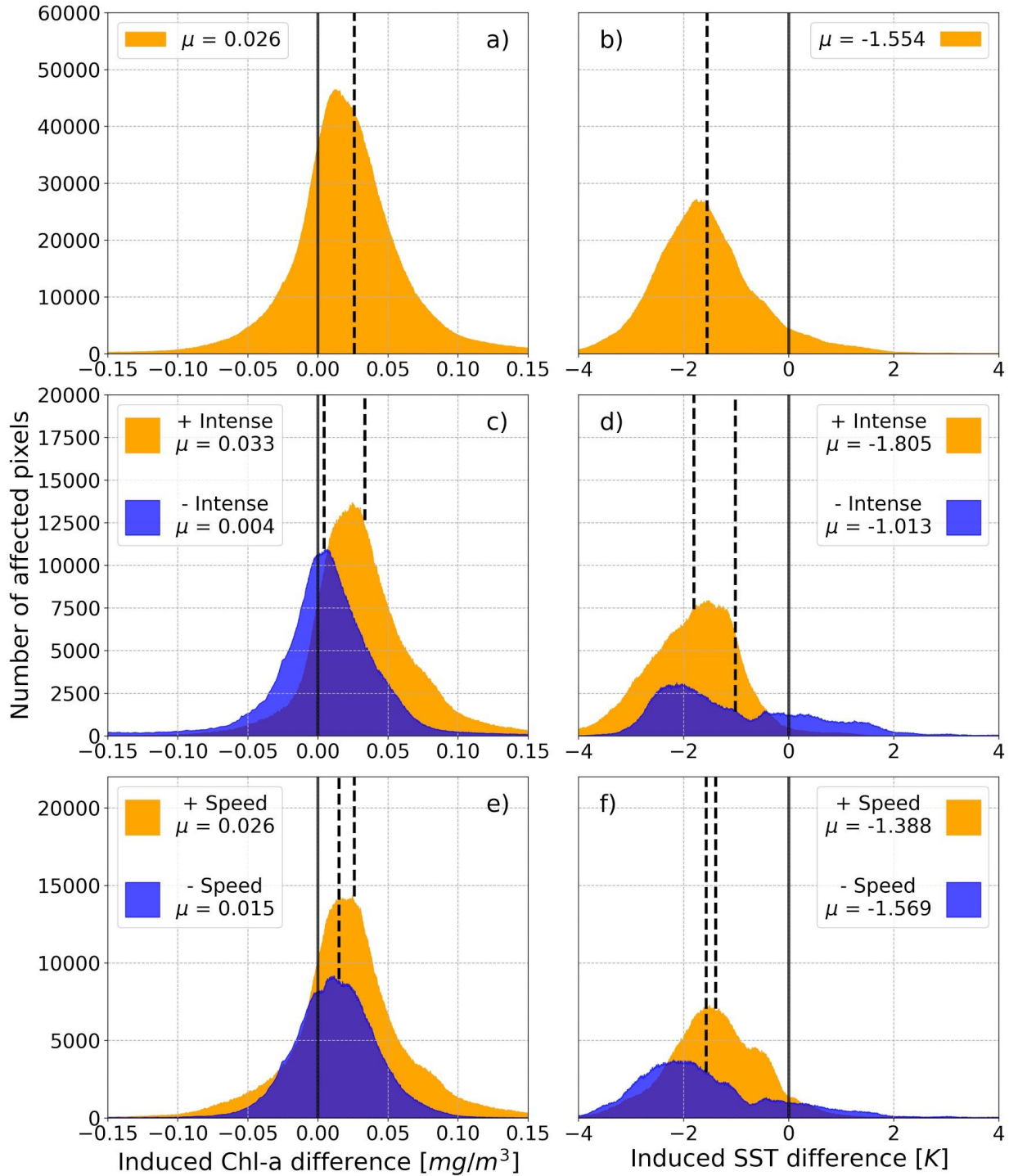
238 [As previously mentioned in the Data section, the interpolated data used for this study is expected to encounter some](#)
 239 [regions where clouds are to be expected due to the presence of the TCs. To account for this potential caveat, we looked](#)
 240 [at the uncertainties associated with the data before and after the TCs, as well as during the TC \(e.g., day 0 in Fig. 2\),](#)
 241 [to evaluate if there were clear increases in uncertainty for cloud covered situations.](#)

242 [Two case studies were looked at in greater detail: Hurricane Ophelia \(2017\) and Hurricane Nadine \(2012\). The former](#)
 243 [was performed to assess the different impacts along the lifecycle of the storm, and different histograms were produced](#)
 244 [for smaller portions of the TC. The latter was made to analyse the possible increasing impacts the storm geometry](#)
 245 [could cause. Additionally, these study cases were used as validation for the interpolated “cloud-free” data, where a](#)
 246 [comparison was made between the non-interpolated and the interpolated “cloud-free” data described in the Data](#)
 247 [section.](#)

248 Results and Discussion

249 Applying the mentioned methodology leaves us with a large pool of induced anomalies, from which we can now
 250 evaluate the distribution of anomalies for both the [chlChl-a](#) and SST as shown in Figs. [4a3a](#) and [4b3b](#) in the form of
 251 histograms of induced [chlChl-a](#) and SST anomalies, respectively. Both variables [suffered present](#) a large impact after

252 the passage of TCs, with the chlChl-a presenting a mean response of positive $0.026050 \text{ mg/m}^3 \text{ m}^{-3}$ and the SST
 253 showing a mean response of negative 1.554615 K . Figs. 4e3c-f show the corresponding distributions as a function of
 254 the cyclone's intensities (Figs. 4e3c and 4d3d) and translation speeds (Figs. 4e3e and 4f3f). To make these distinctions,
 255 we chose only the high values (either regarding intensity or translation speed) to be those above the third quartile and
 256 the lower values to be those below the second quartile.

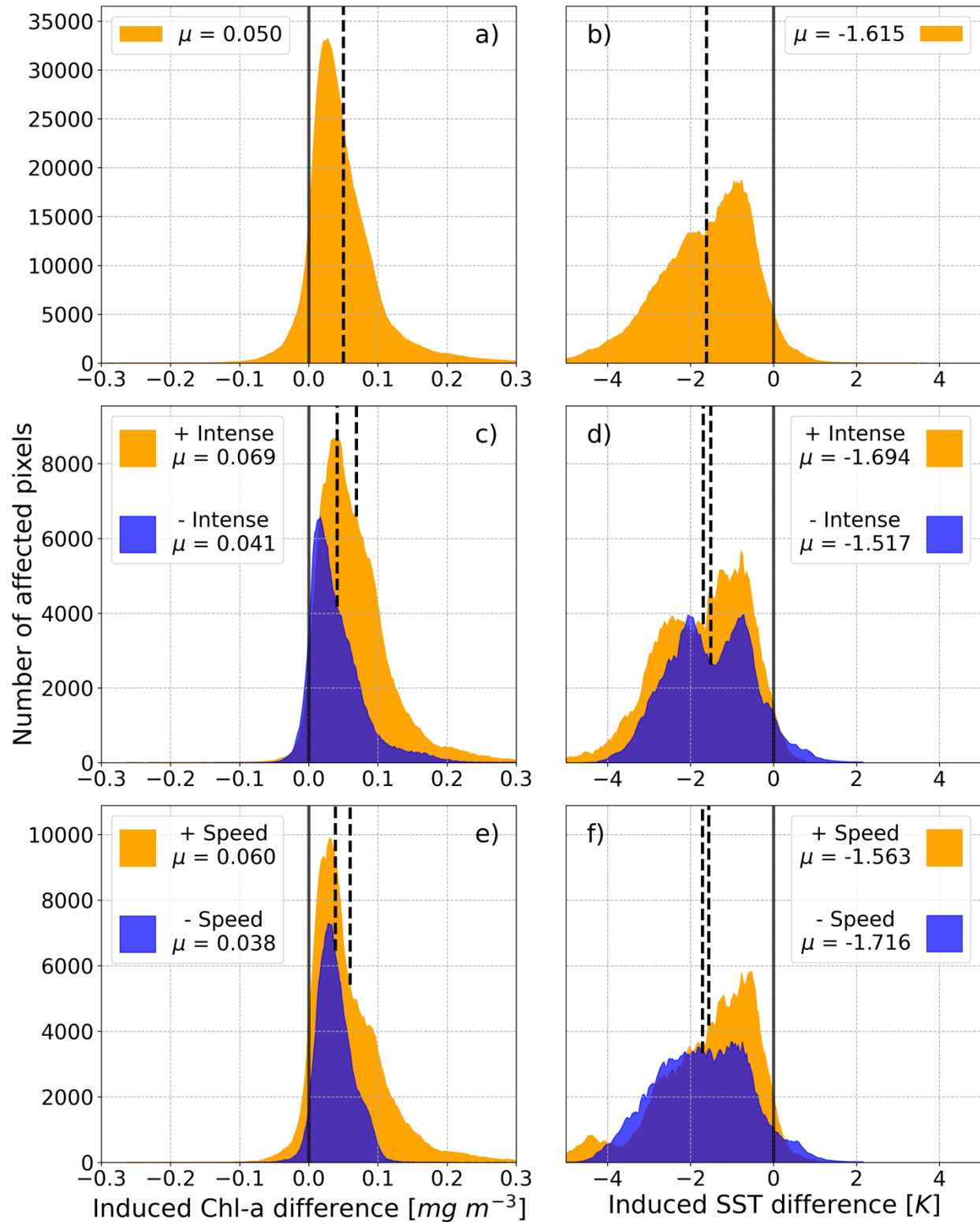


257

258 ~~Figure 4—Histograms for the: a) Total chl-a and b) SST induced anomalies; c) Chl-a and d) SST induced anomalies after~~
259 ~~weaker (blue) and powerful TCs (orange); e) Chl-a and f) SST induced anomalies after slow TCs (blue) and fast TCs~~
260 ~~(orange). Each subplot histogram presents the respective population mean value (μ) in a dashed black line, and the zero~~
261 ~~value on a grey line.~~

262 Firstly, regarding intensity (Figs. 4e3c and 4d3d), we have the induced response of the most powerful intensities in
263 orange and the weaker ones in blue. Regarding the impact as a function of intensity it is possible to observe that more
264 powerful TCs tend to induce a stronger biological response than weaker ones, which have a mean response ~~much~~
265 closer to zero. It is also important to note that the more powerful TCs have a response that is much more skewed
266 towards extreme positive values of ~~chlChl-a~~. Fig. 4d,3d also shows a ~~much larger~~ great impact regarding different
267 intensities in SST, in which even weaker TCs show a substantial mean response of -1.013517 K and nearly all the
268 analysed pixels showing negative induced anomalies. Important to note the nearly bimodal nature of this distribution,
269 which can be attributed to both the earlier phase of TCs (more energy being drawn from the ocean) resulting in more
270 negative SST values, and the less negative corresponding to the ~~latter~~ later part of TCs since baroclinic instabilities are
271 more prevalent than the action of moist enthalpy flux from the ocean at this phase (Baatsen et al., 2015; Emanuel,
272 2003). Powerful TCs induced a more varied distribution of anomalies, with a mean response of -1.805 K. ~~Do note that~~
273 ~~these different distributions do not represent the same geographical areas, since they are analysing different~~
274 ~~observations associated with the location of each TC as it moves along its storm track~~694 K.

275 Regarding the different translation speeds, Fig. 4e3e shows that, for biological responses, ~~this categorization~~ faster
276 TCs show a greater mean value of +0.060 mg m⁻³. This difference is not as ~~important since they present similar mean~~
277 responses, close to ~~expressive as~~ the general one seen in Fig. 4a, with faster TCs showing a slightly larger mean
278 value.3c. On the other hand, the SST response (Fig. 4f3f) seems to be ~~weakly~~ impacted by the TC's translation speed,
279 with slower TCs ~~having~~ have a ~~slightly~~ stronger impact than faster ones. ~~Even though, while~~ the mean response values
280 do not differ as much as the ones in Fig. 4d, ~~these distributions show relatively greater deviations~~3d. Additionally,
281 even if faster TCs do not affect the SST response as much as slower ones, the mean value is still close to what is seen
282 in the general case in Fig. 4b3b, and most of the impact is towards negative SSTs.



283

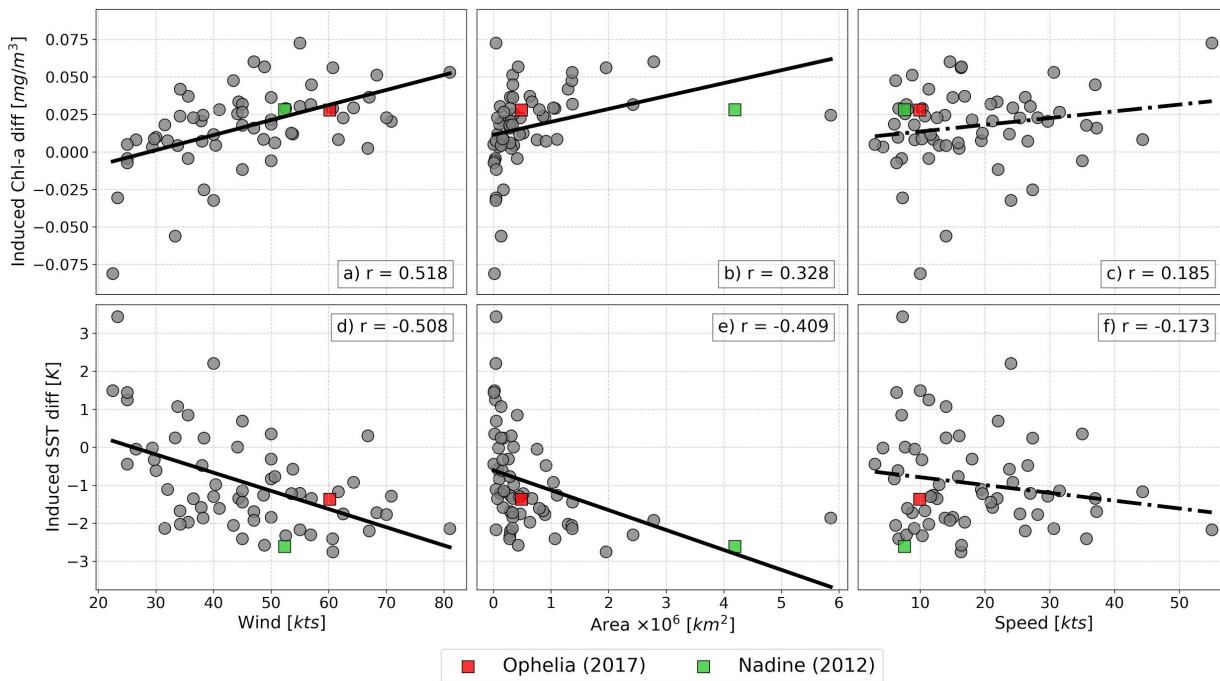
284

285

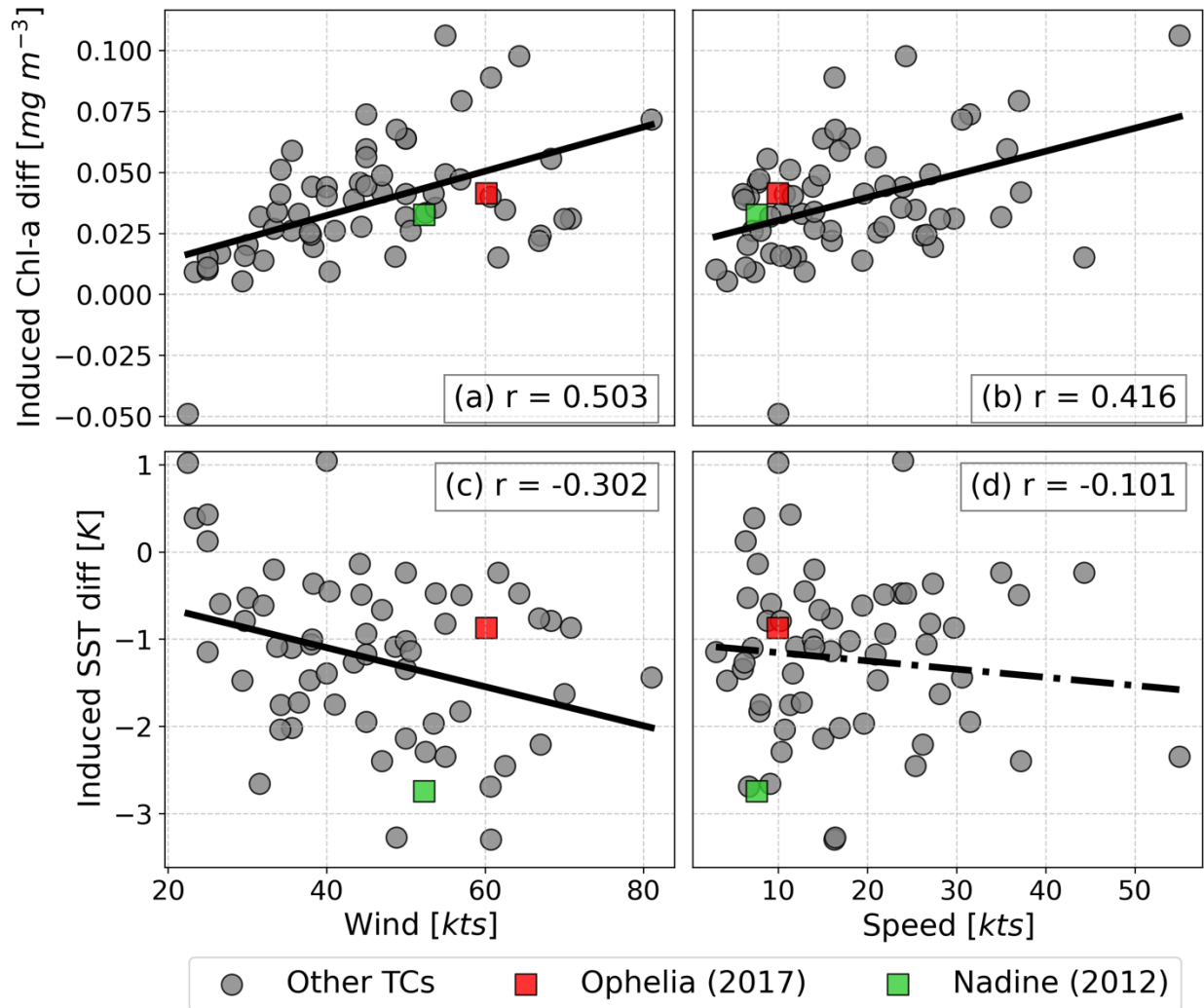
Figure 3 - Histograms for the: a) Total Chl-a and b) SST induced anomalies; c) Chl-a and d) SST induced anomalies after weak (blue) and powerful TCs (orange); e) Chl-a and f) SST induced anomalies after slow TCs (blue) and fast TCs (orange).

286 Each subplot histogram presents the respective population mean value (μ) in a dashed black line, and the zero value on a
 287 grey line.

288 To quantify these relations, Fig. 54 shows the storm-averaged induced anomalies compared to the averaged maximum
 289 wind, cumulative impacted area, and average translation speed. The linear regression is also shown for each of the
 290 comparisons, with nearly all results significant at the 95 % statistical level except for those in the last column
 291 (regression line dashed). According to these plots, only the translation speed in relation to the SST induced anomalies
 292 (Figs. 5e and 5f4d) did not show a significant relation with the chl-a and SST induced anomalies, at the 95 % statistical
 293 confidence level (marked by the dashed regression line). Regarding the mean wind (Figs. 5a4a and 5d4c), and
 294 therefore the TC's average intensity within the Azores region, the linear regression showed significantly high values,
 295 upwards of 0.5, for Chl-a and -0.3 for SST induced anomalies. In the case of chl-a, like observed in Fig. 43, the
 296 relation is positive while with SST this relation is negative. The cumulative area (Figs. 5b and 5e) also presents a
 297 significant relation, although less intense than that observed with Considering the mean winds. However, it should be
 298 noted that this variable is somewhat connected with the mean winds, since more intense eyelones tend to be larger
 299 than less powerful ones, but also with the storm phase, since storms nearing their post-tropical transition tend to grow
 300 larger (Knaff et al., 2014). It is then relatively straightforward that, in the Azores region, the variable that better relates
 301 the bio-physical oceanic response to the passage of a TC is its intensity (Figs. 4 and 5), and to a lesser degree its
 302 translation speed (Fig. 4, the relation is equally positive and significant for biological responses ($r = 0.416$)).



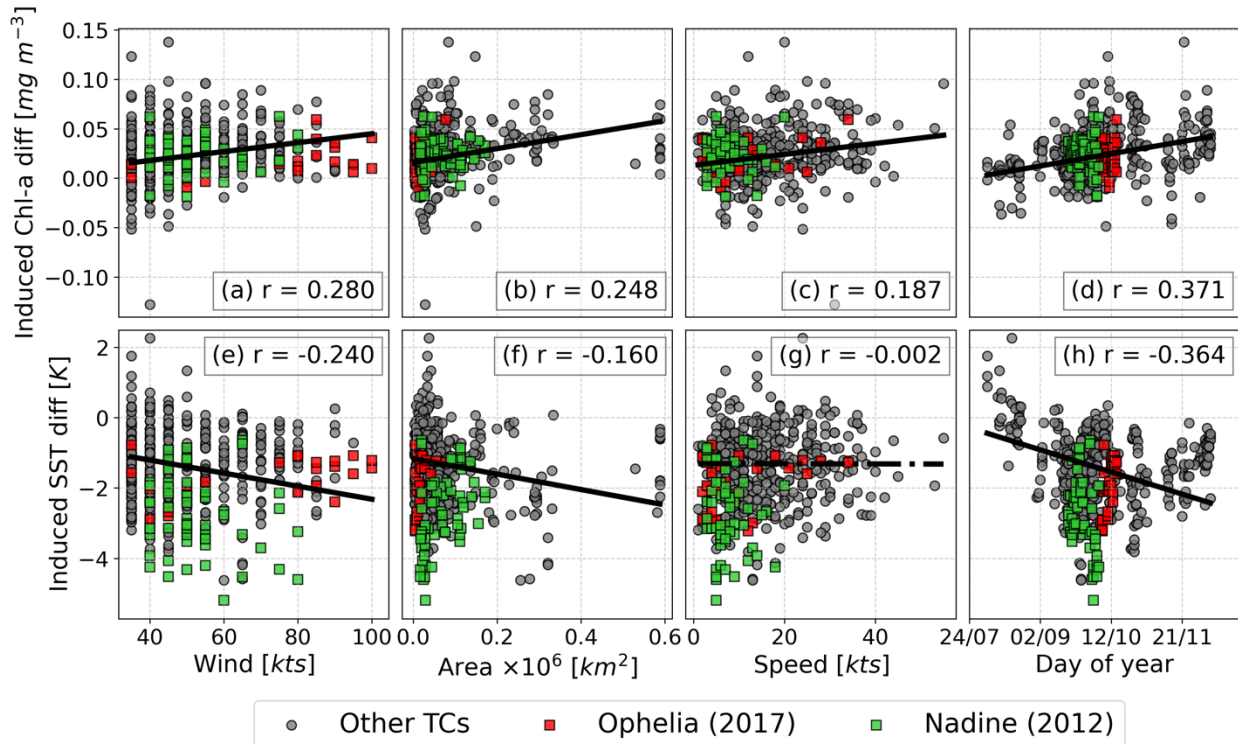
303



304

305 **Figure 54** - Linear regression of ~~chl~~Chl-a (top panel) and SST (bottom panel) induced anomalies for each TC, respectively,
 306 when compared with: average winds in knots (left column); cumulative impacted area in km² (middle column); and average
 307 TC translation speed in knots (right column). In each plot the Pearson R is presented, and the regression's significance is
 308 marked by the type of line used in the regression, with a dashed line representing non-significant at a 95 % confidence
 309 level, and a solid line representing a regression significant at the 95 % confidence level.

310 Further analysis of other TC characteristics requires a different approach, Fig. 5 shows similar relations to Fig. 4, but
 311 considering 6-hour observations instead of total TC mean values. This is made to account for the possible error that
 312 averaging a whole TC may create since the cyclone's characteristics may change substantially along its lifetime. This
 313 analysis, however, does not consider the possibility of superposition in pixels from observation to observation – i.e.,
 314 from a TC that either moves slowly or whose track is more erratic, ending up covering the same area for several
 315 hours/days. This caveat was not present in Fig. 4 since we considered the TC lifetime as a whole and could then
 316 disregard the days of superposition. Using 6-hour observations, we can study several types of characteristics that
 317 change between observations, such as the impact area or the time of season when it occurred, adding to the already
 318 seen maximum wind speed and translation speed.

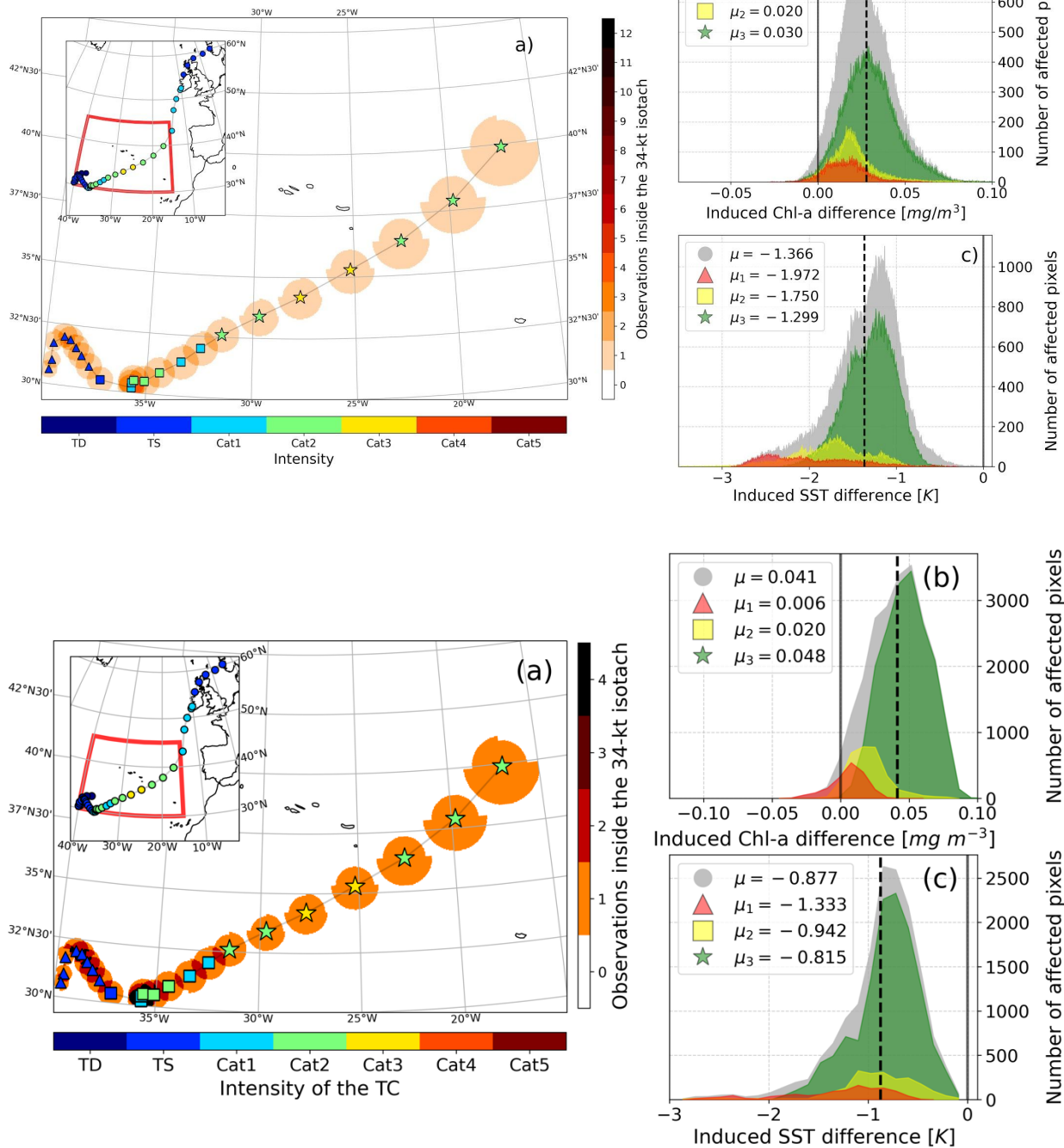


319
 320 **Figure 5**—Same as in Fig. 5 but considering individual 6-hour observations. Two columns are added: (b) and (f) with respect
 321 to the area affected by that observation; and (d) and (h) with respect to the time of the season when that observation
 322 occurred.

323 Considering then the maximum wind speed per observation (Fig. 5a and 5e), both variables are significantly related
 324 to this characteristic, which is expected considering the analysis made in Figs. 3 and 4. As previously noted in the
 325 form of histograms in Fig. 3, most observations show a positive impact regarding Chl-a and, especially for SST as
 326 most fall below zero, a negative change after a TC. The affected area (Figs. 5b and 5f) also presents a significant
 327 relation, although less intense than that observed with the maximum winds. However, it should be noted that this
 328 variable is linked to the mean winds, since more intense cyclones tend to be larger than less powerful ones, but also
 329 to the storm phase, since storms nearing their post-tropical transition tend to grow larger (Knaff et al., 2014). Still in
 330 Fig. 5, two case studies are marked: Hurricane Ophelia in 2017 (red square) and Hurricane Nadine in 2012 (green
 331 square). Translation speed is the less correlated variable from those studied (Fig. 5c and 5g), with only the biological
 332 response seeing a positive relation to this characteristic, agreeing with the previous results from Figs. 3 and 4. The
 333 time period in the season in which the TC occurs seems to also be important for the magnitude of the average induced
 334 anomaly seen in both variables (Figs. 5d and 5h) with late occurrences in the season showing greater responses
 335 respective to the signal of induced anomalies seen in Figs. 3a and 3b. Lastly, a geographical correlation was concluded
 336 not to be relevant for this study (not shown), as both variables were correlated with both latitude and longitude, and
 337 only negligible and non-significant relations were found.

338 The results presented so far in this study result from interpolated “cloud-free” data and should be quality assured to
339 guarantee the integrity of the conclusions made previously. As mentioned in the *Data* section, CMEMS provides
340 measures of uncertainty for the used Chl-a and SST datasets, thus, we have explored these values at different periods
341 as a first step in validating the quality of the data. Figure S1 shows the associated uncertainty with respect to the
342 absolute observed values both for Chl-a (top panels) and SST (bottom panels) for three different periods surrounding
343 a TC event (before, during, and after), and a randomly drawn sample of the same size as the data analysed in the other
344 subplots. It becomes immediately clear from these plots the considerably different magnitude of uncertainty for this
345 data, with Chl-a (Figs. S1a-d) ranging from 25 % to 45 % considering all moments, while SST (Fig. S1e-h) does not
346 commonly surpass 0.4 % with a mean error around the 0.25 %. The randomly drawn sample of data gives a rough
347 idea of the average uncertainty we can find in this dataset, with Chl-a (Fig. S1a) presenting values around 35 % and
348 SST (Fig. S1e) around 0.25 %. Additionally, we should consider three distinct moments of analysis, namely before
349 and after the TC passage, which corresponds to the data used to compute the induced anomalies, and during the TCs,
350 which should be the moment with most cloud-cover over the studied regions. Looking first at Chl-a (Figs. S1b-d) we
351 see the progression from near normal uncertainty before the TC (Fig. S1b) to an increase during TCs (Figs. S1c),
352 maybe due to the higher cloud-covered area in this situation, after the storm (Fig. S1d) however, the uncertainty
353 substantially decreases reaching values below the randomly drawn sample (around 30 % compared to 35 %). For the
354 SST (Figs. S1f-h), the associated uncertainty does not fluctuate substantially, constantly being below the 0.3 % mark.
355 Additionally, it is noticeable in both variables the variation that has been identified before, with Chl-a increasing and
356 the SST decreasing.

357 Visible in Figs. 4 and 5 are two case studies are marked: Hurricane Ophelia in 2017 (red squares) and Hurricane
358 Nadine in 2012 (green squares). These case studies were chosen based on the presented characteristics, coupled with
359 the amount of sampling data within the region. Hurricane Ophelia (2017) was chosen due to its large intensity in the
360 region (Red square insquares, Fig. 4 and 5), reaching a category 3 intensity in the Saffir-Simpson hurricane wind scale,
361 something abnormal for the region (Lima *et al.*, 2021). The complete TC track can be seen in Fig. 6a inset. Besides
362 the large intensity, Ophelia’s genesis took place inside our sectorstudy region which enabled us to study different
363 phases of the storm and its impacts on the ocean surface in the region. Even though hurricane Ophelia was so intense,
364 this storm impacted a very small area (Figs. 5b and ~~5e5f~~) particularly when compared with the other case study,
365 Hurricane Nadine (2012). Hurricane Nadine (Fig. 7a) was chosen due to its large sampling, relatively high intensity
366 (maximum category 1) and massivegreat impact area (second largesthighest in this study), considering cumulative
367 area of impact). The large, impacted area was amplified by the geometry of the storm's track (i.e., many overlaid
368 observations). Only the final stage of Hurricane Nadine was caught within the study region, producing an ideal case
369 study to analyse the impact of a less intense storm that heavily impacted a particular region due to its geometry.

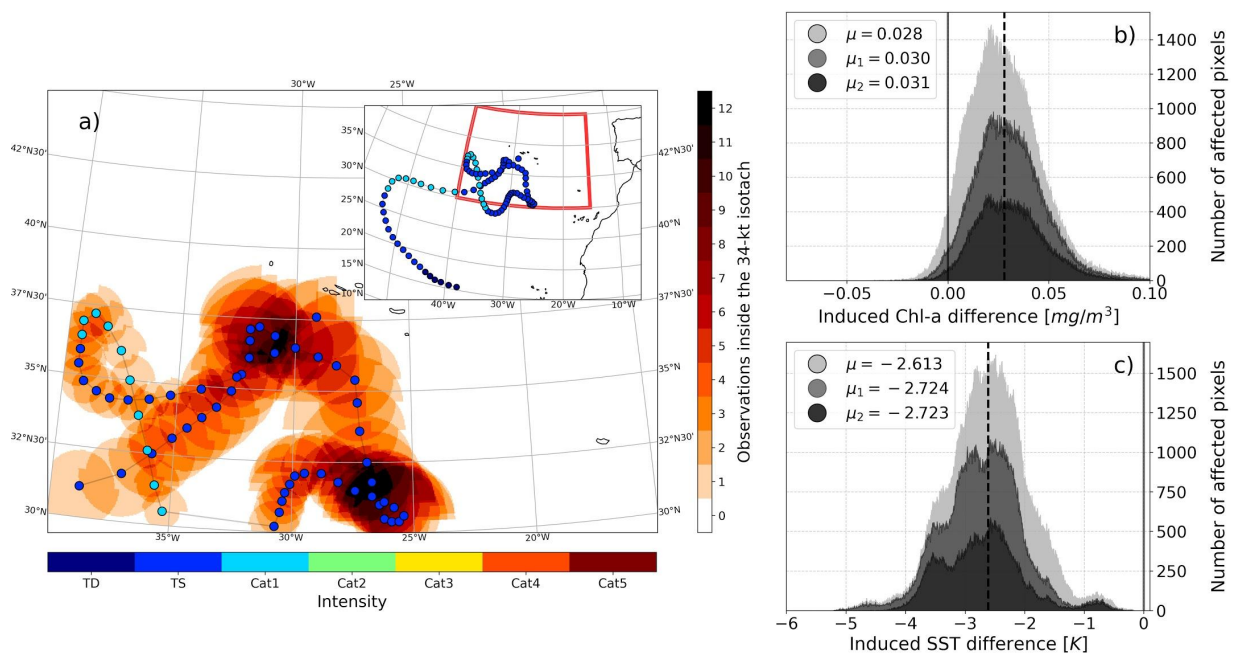


370

371

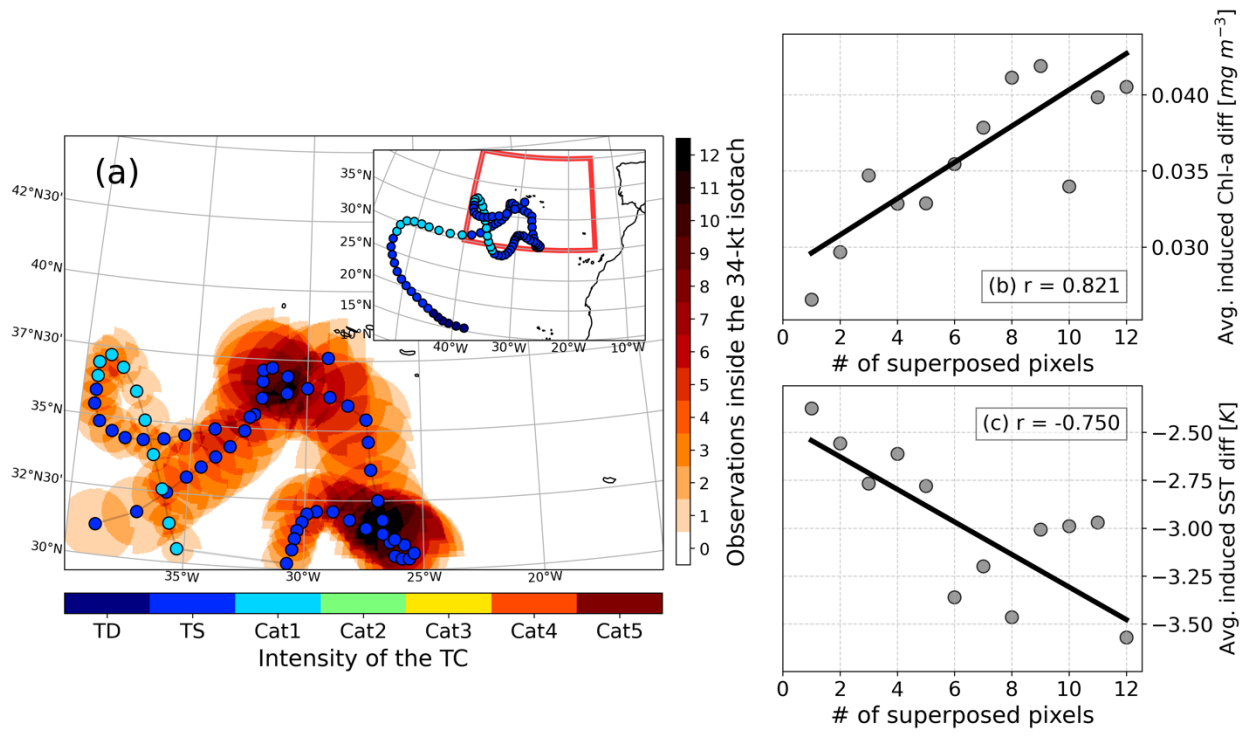
372 Figure 6 - Case study for Hurricane Ophelia, in 2017, with its track on the left panel (intensity-scatter marker colour scheme
 373 represents intensity as in Fig. 21), as well as the affected area around the cyclone (marked as the 34-kt isotach) with shading
 374 according to the number of pixels overlapping. Inside, there is an inset with the full track and the region of study marked
 375 with a red box. Ophelia track is divided in three phases: Genesis (triangles), maturing (squares) and mature (stars).
 376 Histograms show induced chlChl-a (b) and SST anomalies (c), by phase of the storm (colours) and generalin total (grey).
 377 The phase of the storm is marked in (a) as triangles (genesis), squares (maturing), and stars (mature) and correspond to
 378 the aforementioned colours in (b) and (c).

379 For the case study of Hurricane Ophelia (2017), three different phases of the storm were studied, corresponding
 380 approximately to: cyclogenesis (Fig. 6a, triangles), maturing (Fig. 6a, squares), and mature hurricane (Fig. 6a, stars).
 381 There are 23 total observations; the first two phases encompass 8 observations and the last one 7. Each of these phases
 382 has its own histogram in Figs. 6b and 6c (shown in colours), for the induced chlChl-a and SST anomalies, respectively.
 383 The histograms are inserted in a larger one (in grey), representing the total induced anomalies caused by Ophelia and
 384 therefore, the sum of all three phases will result in the bigger one histogram. Regarding the chlChl-a induced anomalies
 385 (Fig. 6b), Ophelia seemed to have a higher impact towards the end of its track in the region of study, when the storm
 386 had the highest intensity and the mean values of the induced anomalies increased along the track. Even at the storm's
 387 genesis, the induced anomalies were mostly positive with a mean value of +0.016006 mg/m^3 reaching +0.030048
 388 mg/m^3 in the most intense phase. In contrast, the SST induced anomalies (Fig. 6c) present the highest mean
 389 response (-1.972333 K) at the initial phase. The SST induced anomaly is then seen decreasing as the storm goes on,
 390 with the last phase weighing the most in the general distribution (as was seen for the chlChl-a). The highest SST
 391 impact of the storm during the initial phases may reflect that this is the phase of the storm with highest interaction
 392 with the ocean, regarding thermodynamic exchanges (Emanuel, 2003).



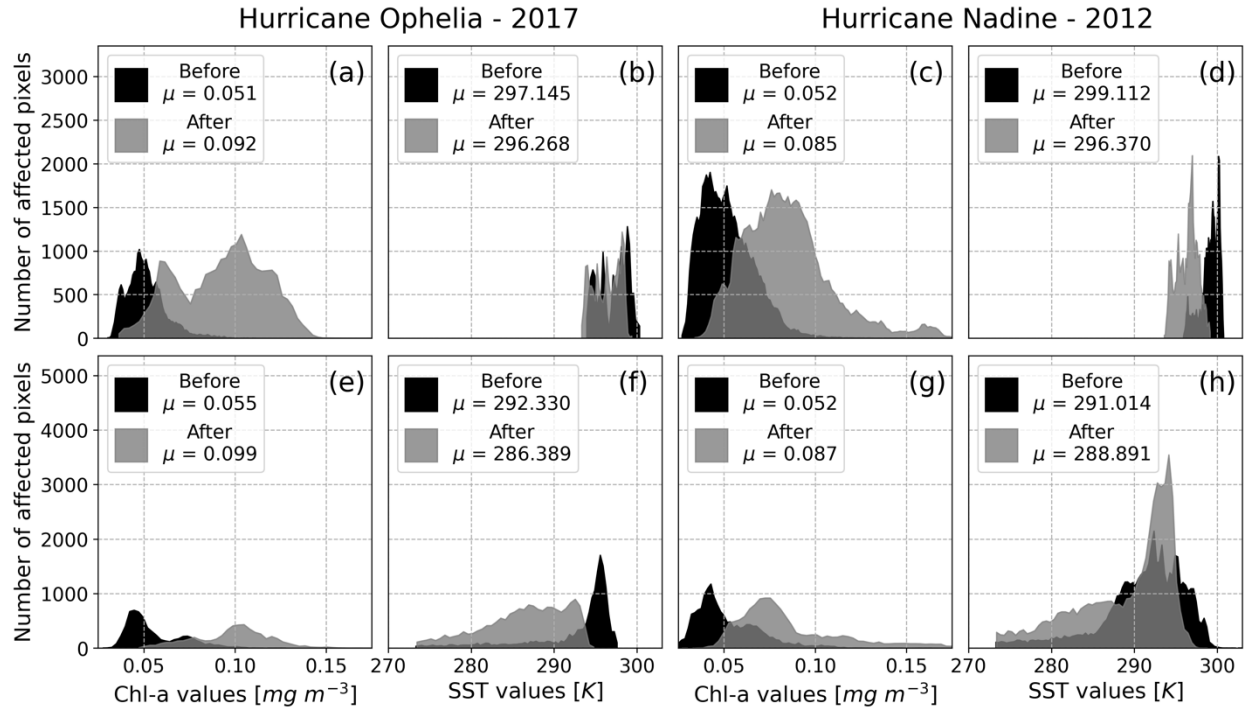
393
 394 As a further insight to Ophelia's interaction with the ocean surface, Fig. S3 shows the mean modulus of wind stress
 395 on the surface, by day of analysis (Fig. S2a) and by Ophelia's 6-hour observations (Fig. S2b). Marked in both these
 396 plots are the analysed periods in corresponding colours and marker type to Fig. 6, these plots exceed the original study
 397 region, in order to fully encompass the TCs entire lifetime. There is a significant relation between the increased mean
 398 modulus of the wind stress and the evolution of the TC in time. This increase may be related to the increase in the
 399 storm's intensity, as Ophelia reaches its maximum intensity, so does the observed interaction with the ocean,
 400 decreasing afterwards as the storm moves north-eastward and undergoes post-tropical transition. This observed

401 interaction with the ocean might be the reason for the maximum induced anomaly of Chl-a being observed at the end
 402 of Ophelia's passage over the study region, inducing the mixing of the superficial layer.



403
 404 **Figure 7 - Case study for Hurricane Nadine, in 2012, with the rightleft panel the same as in Fig. 6. For Nadine, histograms**
 405 **plots (b) and (c) pertain to the average induced chlChl-a and SST anomalies, respectively, based on the amount of**
 406 **overlapsuperposition verified in each pixel: soft grey No overlap; Dark grey 3-pixel overlap; Black 5-pixel overlap.**

407 Hurricane Nadine's (2012) case study shows very different behaviour and impact during its lifetime to that of
 408 Hurricane Ophelia. In this case, histograms represent differently impacted areas, with we present scatter plots of the
 409 darker histograms averaged induced anomalies for the areas (Figs. 7b and 7c) corresponding to the areas with more
 410 overlaid superposition of pixels, i.e., the number of repeated observations inside the 34-kt isotach due to storms track
 411 geometry (as seen in Fig. 7a). The threshold chosen for analysis were 3 overlaid observations for the middle shade
 412 and 5 for the darkest one, with the biggest histogram showing the general induced anomalies for Hurricane Nadine.
 413 The conclusions drawn regarding the chlChl-a and SST induced anomalies are similar and significant in this case
 414 study: The more time the TC spent over a certain area the more this area became affected by its passage, with large
 415 anomalies registered in both variables (over 0.031040 mg/m³ m⁻³ and -2.7233.500 K for chlChl-a and SST,
 416 respectively). This shows that the TC intensity is somewhat irrelevant given that the geometry of its track is ideal to
 417 stay longer over), and all cases being positive (negative), for Chl-a region. With this in mind, it(SST). It is possible
 418 to hypothesise that the translation speed also had a relevant role in these results, with a slower TC (Nadine was one of
 419 the slowest TCs in this study, as seen by the closer observations in Fig. 7a and by Figs. 5e4 and 5f5) spending more
 420 time over a region and therefore producing larger anomalies.



421

422 **Figure 8 – Comparison between interpolated “cloud-free” data (top row), and non-interpolated data (bottom row), for**
 423 **Hurricanes Ophelia (2017) and Nadine (2012). Values for non-interpolated data were obtained with the same methodology**
 424 **as the ones presented before and represent the exact same days of analysis. Mean values for each histogram are presented,**
 425 **with black histograms representing the situation before the TC and the grey ones the situation after.**

426 For these two case studies, we considered an additional quality assessment exercise, by comparing the interpolated
 427 “cloud-free” data to similar non-interpolated datasets. Figure 8 shows the histograms obtained for Ophelia and Nadine
 428 for the situations before and after the TC, independently, since non-interpolated data cannot be correctly subtracted as
 429 corresponding pixels may not be available. Overall, and despite the different number of observations considered, the
 430 Chl-a presents the same average response between the different types of data for both TCs, with non-interpolated data
 431 having an observed mean increase of $0.044\ mg\ m^{-3}$ for Ophelia (Fig. 8e) compared to $0.041\ mg\ m^{-3}$ for interpolated
 432 data (Fig. 8a), with these values representing the difference in the mean values shown in Fig. 8. Likewise, non-
 433 interpolated data reveals an increase of $0.035\ mg\ m^{-3}$ for Nadine (Fig. 8g), compared to $0.033\ mg\ m^{-3}$ for interpolated
 434 data (Fig. 8c). Looking at the histograms, the shape of the data itself does not differ too much between the different
 435 types, with peaks more or less located over the same values and distributions ranging the same values. However, for
 436 the SST variable, despite both TC’s present relatively similar decreases between both types of data, the non-
 437 interpolated data has a wider range of values, and the peaks do not correspond so closely. This, however, may be due
 438 to the process of data collation. In this process, some pixels are averaged with incorrect ones, resulting in unrealistic
 439 values in some areas. This can be identified by the unrealistic SST seen in Figs. 8f and 8h, with values that do not
 440 support TC development around $18-19^{\circ}C$ and, so far as reaching $0^{\circ}C$. Nonetheless, interpolated SST data does show
 441 the less uncertainty as verified before as the process of interpolating the data fixes this issue (Fig. S1).

442 **Final remarks**

443 The current study provides the first general assessment of the bio-physical oceanic response to the passage of TCs in
444 a relatively low cyclonic activity area such as the region near the Azores archipelago. It is important to stress the
445 efficiency of identifying the precise timing and associated spatial impacts of all TCs using remotely sensed products
446 that rely on interpolated areas to fill existing gaps due to cloud coverage or lack of satellite imagery.

447 Over the Azores region, it was generally identified the existence of a bio-physical response after the passage of a TC
448 was identified from the analysis of chl-a and SST datasets, which produced signatures of positive (chl-a) and
449 negative (SST) induced anomalies, for a period of about two weeks after the passage of a TC. This signature is
450 considerably more intense for the SST analysis, in which the passage of a TC results in nearly all observed pixels to
451 have a negative (i.e., cooling) induced anomaly. On average, TCs produced positive anomalies in the order of 0.026050
452 mg/m³ m⁻³ regarding chl-a and a mean SST cooling of 1.554615 K.

453 The more powerful TCs tend to produce more intense bio-physical oceanic responses, which agree with previous
454 literature on the topic (Chacko, 2019; Price, 1981; Price et al., 1994). The TCs translation speed was also
455 confirmed to be relevant in inducing associated with the induced anomalies in both variables, although in this
456 instance the direct relation was not confirmed since results were not the relationship was found to be positive and
457 significant in the case of Chl-a while it was not significant at the 95 % statistical confidence level for SST. The
458 impacted area was also found to be significantly linked to the oceanic response. However, the sensitivity to the
459 impacted area can rise due to several other factors: slower TCs impact larger areas (due to track geometry); more
460 intense TCs impact larger areas (Knaff et al., 2014); and TCs nearing post-tropical transition are generally larger
461 (Knaff et al., 2014). These effects, either individually or combined, can affect the induced anomalies at different
462 levels. Additionally, the oceanic response was found to be increased later in the season, with significant relation in
463 both variables, this may be due to the seasonal variability of the variables themselves, as the normal climatological
464 values for that time of the year is exceeded in exceptional TC conditions (Amorim et al., 2017; Lima et al., 2021) and
465 the oceanic response may help the impacted area return to expected values in both variables, in respect to that time of
466 the year.

467 Two particular case studies were evaluated in further detail concerning hurricanes Ophelia (2017) and Nadine (2012).
468 Hurricane Ophelia was a particular case as it corresponds to the only major hurricane in this study region and had
469 almost its entire track inside this area. Ophelia showed strong induced anomalies for both chl-a and SST variables.
470 Regarding chl-a, Ophelia had a stronger impact towards the end of its track within the region, revealing that its
471 intensity played a key role in inducing chl-a anomalies. Chl-a anomalies, with the mean modulus of wind stress
472 revealing a positive and significative relation to the evolution of the storm and therefore its intensity. On the other
473 hand, Ophelia had a stronger impact on the SST in its cyclogenesis, probably related to ocean-atmosphere
474 thermodynamic exchanges during its maturing. Hurricane Nadine, one of the slowest TCs in this study, showed more
475 prominent anomalies, especially regarding SST. In this case, considering the low translational speed of Nadine, the
476 objective was to study the impact that consecutive overlaid observations had on the induced anomalies. It is evident

477 through this analysis that the impact increases with the number of ~~overlaid~~superposed observations, implying that
478 Nadine's slow translation speed and particular track geometry played a key role in creating such anomalies.

479 This study allowed for both the quality control of the remotely sensed "cloud-free" ~~chl~~Chl-a and SST multi-sensor
480 products; by comparing them to similar non-interpolated products, and in the sense that it identified expected changes
481 in the variables in areas covered by TC clouds and established crucial relations with some principal TC aspects. Future
482 studies should aim to understand the inherent physical mechanisms that affect the ocean during and after the passage
483 of a TC to better comprehend the associated induced anomalies.

484 **Code and Data availability**

485 All code and raw data used to support the conclusion of this article will be made available by the authors, without
486 undue reservation.

487 **Acknowledgements**

488 Research by Miguel M. Lima was supported by the Portuguese Science Foundation (FCT) through the project
489 "DiscoverAZORES", PTDC/CTA-AMB/28511/2017. The authors would like to thank the anonymous reviewers for
490 their thoughtful comments, suggestions, and efforts towards improving this work.

491 **Author Contribution**

492 Miguel M. Lima: Conceptualization, methodology, software, validation, formal analysis, investigation, writing –
493 original draft, review ~~&~~and editing. Célia M. Gouveia: Validation, supervision, writing – review ~~&~~and editing.
494 Ricardo M. Trigo: Validation, supervision, writing – review ~~&~~and editing, funding acquisition.

495 **Declaration of Interests**

496 The authors declare that they have no known competing financial interests or personal relationships that could have
497 appeared to influence the work reported in this paper.

498 **References**

- 499 Amorim, P., Perán, A. D., Pham, C. K., Juliano, M., Cardigos, F., Tempera, F., ~~&~~and Morato, T. ~~(2017)~~.: Overview
500 of the ocean climatology and its variability in the Azores region of the North Atlantic including environmental
501 characteristics at the seabed. Frontiers in Marine Science, 4, 56. doi:10.3389/fmars.2017.00056, 2017.
- 502 Baatsen, M., Haarsma, R. J., Van Delden, A. J., and de Vries, H. ~~(2015)~~.: Severe Autumn Storms in Future Western
503 Europe with a Warmer Atlantic Ocean. Clim. Dyn. 45 (3-4), 949–964. doi:10.1007/s00382-014-2329-8, 2015.

504 [Celisse, A., Marot, G., Pierre Jean, M., & Rigail, G. J. \(2018\). New efficient algorithms for multiple change point](#)
505 [detection with reproducing kernels. *Computational Statistics & Data Analysis*, 128, 200-220.](#)
506 [doi:10.1016/j.esda.2018.07.002](#)

507 [Caldeira, R., and Reis, J. C.: The Azores confluence zone. *Frontiers in Marine Science*, 4, 37,](#)
508 [doi:10.3389/fmars.2017.00037, 2017.](#)

509 Chen, S., Elsberry, R. L., ~~&and~~ Harr, P. A. (2017). ~~Modeling~~~~A.:~~ ~~Modelling~~ interaction of a tropical cyclone with its
510 cold wake. ~~*Journal of the Atmospheric Sciences*, *J. Atmos. Sci.*~~, 74(12), 3981-4001, doi:10.1175/JAS-D-16-0246.1,
511 [2017.](#)

512 Chacko, N. ~~(2019)~~. Differential chlorophyll blooms induced by tropical cyclones and their relation to cyclone
513 characteristics and ocean pre-conditions in the Indian Ocean. ~~*Journal of*~~ *Earth System Science, Syst. Sci.*, 128(7), 1-
514 11. doi:10.1007/s12040-019-1207-5, [2019.](#)

515 CMEMS. ~~(2021a)~~: ESA SST CCI and C3S reprocessed sea surface temperature analyses. Retrieved from
516 [https://resources.marine.copernicus.eu/?option=com_csw&view=details&product_id=SST_GLO_SST_L4_REP_O](https://resources.marine.copernicus.eu/?option=com_csw&view=details&product_id=SST_GLO_SST_L4_REP_OBSERVATIONS_010_024)
517 [BSERVATIONS_010_024](https://resources.marine.copernicus.eu/?option=com_csw&view=details&product_id=SST_GLO_SST_L4_REP_OBSERVATIONS_010_024)[https://resources.marine.copernicus.eu/?option=com_csw&view=details&prod](https://resources.marine.copernicus.eu/?option=com_csw&view=details&product_id=SST_GLO_SST_L4_REP_OBSERVATIONS_010_024)
518 [uct_id=SST_GLO_SST_L4_REP_OBSERVATIONS_010_024](https://resources.marine.copernicus.eu/?option=com_csw&view=details&product_id=SST_GLO_SST_L4_REP_OBSERVATIONS_010_024), 2021a.

519 CMEMS. ~~(2021b)~~: Global ocean chlorophyll, PP and PFT (copernicus-globcolour) from satellite observations:
520 Monthly and daily interpolated (reprocessed from 1997). Retrieved from
521 [https://resources.marine.copernicus.eu/?option=com_csw&view=details&product_id=OCEANCOLOUR_GLO_CH](https://resources.marine.copernicus.eu/?option=com_csw&view=details&product_id=OCEANCOLOUR_GLO_CHL_L4_REP_OBSERVATIONS_009_082)
522 [L_L4_REP_OBSERVATIONS_009_082](https://resources.marine.copernicus.eu/?option=com_csw&view=details&product_id=OCEANCOLOUR_GLO_CHL_L4_REP_OBSERVATIONS_009_082), [2021b.](#)

523 Dickey, T., Frye, D., McNeil, J., Manov, D., Nelson, N., Sigurdson, D., ... ~~&and~~ Johnson, R. ~~(1998)~~: Upper-ocean
524 temperature response to Hurricane Felix as measured by the Bermuda Testbed Mooring. ~~*Monthly, Mon. Weather*~~
525 ~~*Review, Rev.*~~, 126(5), 1195-1201, doi:10.1175/1520-0493(1998)126<1195:UOTRTH>2.0.CO;2, [1998.](#)

526 Donlon, C. J., Martin, M., Stark, J., Roberts-Jones, J., Fiedler, E., ~~&and~~ Wimmer, W. ~~(2012)~~: The operational sea
527 surface temperature and sea ice analysis (OSTIA) system. ~~*Remote Sensing of Environment*, *Proc. SPIE*~~, 116, 140-
528 158, doi:10.1016/j.rse.2010.10.017, [2012.](#)

529 Emanuel, K. ~~(2003)~~: Tropical Cyclones. *Annu. Rev. Earth Planet. Sci. Pl. Sc.*, 31 (1), 75-104,
530 doi:10.1146/annurev.earth.31.100901.141259, [2003.](#)

531 Garnesson, P., Mangin, A., Fanton d'Andon, O., Demaria, J., ~~&and~~ Bretagnon, M. ~~(2019)~~: The CMEMS
532 GlobColour chlorophyll a product based on satellite observation: multi-sensor merging and flagging strategies,
533 *Ocean Science, Sci.*, 15(3), 819-830, doi:10.5194/os-15-819-2019, [2019.](#)

534 Good, S., Fiedler, E., Mao, C., Martin, M. J., Maycock, A., Reid, R., ... ~~&and~~ Worsfold, M. ~~(2020)~~.: The current
535 configuration of the OSTIA system for operational production of foundation sea surface temperature and ice
536 concentration analyses. ~~Remote Sensing~~, ~~Sens-Basel~~, 12(4), 720. doi:10.3390/rs12040720, ~~2020~~.

537 Haarsma, R. J., Hazeleger, W., Severijns, C., de Vries, H., Sterl, A., Bintanja, R., ~~et al. (2013)~~.~~...~~ ~~and van den~~
538 ~~Brink, H. W.~~: More Hurricanes to Hit Western Europe Due to Global Warming. ~~Geophys. Res. Lett.~~, 40, 1783–
539 1788. doi:10.1002/grl.50360, ~~2013~~.

540 Hart, R. E., ~~&and~~ Evans, J. L. ~~(2001)~~.: A climatology of the extratropical transition of Atlantic tropical cyclones.
541 ~~Journal of~~, ~~J. Climate~~, 14(4), 546-564. doi:10.1175/1520-0442(2001)014<0546:ACOTET>2.0.CO;2, ~~2001~~.

542 Holton, J. R., and Hakim, G. J. ~~(2012)~~.: An Introduction to Dynamic Meteorology. 5th ed., Vol. 88. San Diego,
543 CA: Academic Press, Elsevier. doi:10.1119/1.1987371, ~~2012~~.

544 Kawai, Y., ~~&and~~ Wada, A. ~~(2011)~~.: Detection of cyclone-induced rapid increases in chlorophyll-a with sea surface
545 cooling in the northwestern Pacific Ocean from a MODIS/SeaWiFS merged satellite chlorophyll product.
546 ~~International journal of remote sensing~~, ~~Int. J. Remote Sens.~~, 32(24), 9455-9471.
547 doi:10.1080/01431161.2011.562252, ~~2011~~.

548 Knaff, J. A., Longmore, S. P., ~~&and~~ Molenaar, D. A. ~~(2014)~~.: An objective satellite-based tropical cyclone size
549 climatology. ~~Journal of~~, ~~J. Climate~~, 27(1), 455-476. doi:10.1175/JCLI-D-13-00096.1, ~~2014~~.

550 Knapp, K. R., Kruk, M. C., Levinson, D. H., Diamond, H. J., and Neumann, C. J. ~~(2010)~~.: The International Best
551 Track Archive for Climate Stewardship (IBTrACS). ~~Bull. Amer.~~, ~~B. Am.~~ Meteorol. Soc., 91 (3), 363–376.
552 doi:10.1175/2009BAMS2755.1, ~~2010~~.

553 Kossin, J. P., Knapp, K. R., Olander, T. L., and Velden, C. S. ~~(2020)~~.: Global Increase in Major Tropical Cyclone
554 Exceedance Probability over the Past Four Decades. ~~Proc. Natl. Acad. Sci. USA~~, 117 (22), 11975–11980.
555 doi:10.1073/pnas.1920849117, ~~2020~~.

556 Krasnopolsky, V., Nadiga, S., Mehra, A., Bayler, E., ~~&and~~ Behringer, D. ~~(2016)~~.: Neural networks technique for
557 filling gaps in satellite measurements: Application to ocean color observations. ~~Computational intelligence and~~
558 ~~neuroscience~~, ~~Comput. Intel. Neurosc.~~, 2016, 29, doi:10.1155/2016/6156513, ~~2016~~.

559 Lavergne, T., Sørensen, A. M., Kern, S., Tonboe, R., Notz, D., Aaboe, S., ... ~~&and~~ Pedersen, L. T. ~~(2019)~~.: Version
560 2 of the EUMETSAT OSI SAF and ESA CCI sea-ice concentration climate data records. ~~The Cryosphere~~, 13(1),
561 49-78. doi:10.5194/tc-13-49-2019, ~~2019~~.

562 Lima, M. M. , Hurduc, A., Ramos, A. M. and Trigo, R. M. ~~(2021)~~.: The Increasing Frequency of Tropical Cyclones
563 in the Northeastern Atlantic Sector. ~~Front. Earth Sci.~~, 9:745115. doi: 10.3389/feart.2021.745115, ~~2021~~.

564 Liu, X., Wang, M., & Shi, W. (2009). A study of a Hurricane Katrina-induced phytoplankton bloom using
565 satellite observations and model simulations. *Journal of Geophysical Research*, *J. Geophys. Res-Oceans*,
566 114(C3), doi:10.1029/2008JC004934, 2009.

567 Maneesha, K., Murty, V. S. N., Ravichandran, M., Lee, T., Yu, W., & McPhaden, M. J. (2012). Upper ocean
568 variability in the Bay of Bengal during the tropical cyclones Nargis and Laila. *Progress in Oceanography*, *Prog.*
569 *Oceanogr.*, 106, 49-61, doi:10.1016/j.pocean.2012.06.006, 2012.

570 Merchant, C. J., Le Borgne, P., Roquet, H., & Legendre, G. (2013). Extended optimal estimation techniques for
571 sea surface temperature from the Spinning Enhanced Visible and Infra-Red Imager (SEVIRI). *Remote Sensing of*
572 *Environment*, *Proc. SPIE*, 131, 287-297, doi:10.1016/j.rse.2012.12.019, 2013.

573 Pan, J., Huang, L., Devlin, A. T., & Lin, H. (2018). Quantification of typhoon-induced phytoplankton blooms
574 using satellite multi-sensor data. *Remote Sensing Sens-Basel*, 10(2), 318, doi:10.3390/rs10020318, 2018.

575 Pearce, R. P. (1987). The physics of hurricanes. *Physics in Technology*, *Phys. Technol.*, 18(5), 215, 1987.

576 Price, J. F. (1981). Upper ocean response to a hurricane. *Journal of Physical Oceanography*, *J. Phys. Oceanogr.*,
577 11(2), 153-175, doi:10.1175/1520-0485(1981)011<0153:UORTAH>2.0.CO;2, 1981.

578 Price, J. F., Sanford, T. B., & Forristall, G. Z. (1994). Forced stage response to a moving hurricane. *Journal of*
579 *Physical Oceanography*, *J. Phys. Oceanogr.*, 24(2), 233-260, doi:10.1175/1520-
580 0485(1994)024<0233:FSRTAM>2.0.CO;2, 1994.

581 Ramsay, H. (2017). The Global Climatology of Tropical Cyclones. Oxford Research Encyclopedia of Natural
582 Hazard Science. Victoria, *Australia Australia*: Oxford University Press,
583 doi:10.1093/acrefore/9780199389407.013.79, 2017.

584 [Saha, K., Zhao, X., Zhang, H., Casey, K. S., Zhang, D., Baker-Yeboah, S., ... and Relph, J. M.: AVHRR Pathfinder](#)
585 [version 5.3 level 3 collated \(L3C\) global 4km sea surface temperature for 1981-Present, NOAA National Centers for](#)
586 [Environmental Information, dataset, doi:10.7289/v52j68xx, 2018.](#)

587 [Sathyendranath, S., Brewin, R. J. W., Brockmann, C., Brotas, V., Calton, B., Chuprin, A., ... and Platt, T.: An](#)
588 [ocean-colour time series for use in climate studies: the experience of the Ocean-Colour Climate Change Initiative](#)
589 [\(OC-CCI\), *AH S. Sens.*, 19\(19\), 4285, doi:10.3390/s19194285, 2019.](#)

590 [Sathyendranath, S., Jackson, T., Brockmann, C., Brotas, V.; Calton, B., Chuprin, A., ... and Platt, T.: ESA Ocean](#)
591 [Colour Climate Change Initiative \(Ocean Colour cci\): Version 5.0 Data, NERC EDS Centre for Environmental](#)
592 [Data Analysis, 19 May 2021, doi:10.5285/1dbe7a109c0244aad713e078fd3059a, 2021.](#)

593 Saulquin, B., Gohin, F., & Fanton d'Andon, O. (2019). Interpolated fields of satellite-derived multi-algorithm
594 chlorophyll-a estimates at global and European scales in the frame of the European Copernicus-Marine Environment

595 Monitoring Service. ~~Journal~~ of ~~Operational Oceanography~~, ~~Oper. Oceanogr.~~, 12(1), 47-57,
596 doi:10.1080/1755876X.2018.1552358, [2019](#).

597 Shropshire, T., Li, Y., ~~&and~~ He, R. ~~(2016)~~: Storm impact on sea surface temperature and chlorophyll a in the Gulf
598 of Mexico and Sargasso Sea based on daily cloud-free satellite data reconstructions. ~~Geophysical Research~~,
599 [Geophys. Res. Letters](#), 43(23), 12-199, doi:10.1002/2016GL071178, [2016](#).

600 Subrahmanyam, B., Rao, K. H., Srinivasa Rao, N., Murty, V. S. N., ~~&and~~ Sharp, R. J. ~~(2002)~~: Influence of a
601 tropical cyclone on chlorophyll-a concentration in the Arabian Sea. ~~Geophysical Research~~, [Geophys. Res. Letters](#),
602 29(22), 22-1, doi:10.1029/2002GL015892, [2002](#).

603 Taylor, H. T., Ward, B., Willis, M., ~~&and~~ Zaleski, W. ~~(2010)~~: The saffir-simpson hurricane wind scale.
604 Atmospheric Administration: Washington, DC, USA., [2010](#).

605 ~~Truong, C., Oudre, L., & Vayatis, N. (2020). Selective review of offline change point detection methods. Signal~~
606 ~~Processing, 167, 107299. doi:10.1016/j.sigpro.2019.107299~~

607 Walker, N. D., Leben, R. R., ~~&and~~ Balasubramanian, S. ~~(2005)~~: Hurricane-forced upwelling and chlorophyll-a
608 enhancement within cold-core cyclones in the Gulf of Mexico. ~~Geophysical Research~~, [Geophys. Res. Letters](#),
609 32(18), doi:10.1029/2005GL023716, [2005](#).

610 Zhang, J., Lin, Y., Chavas, D. R., ~~&and~~ Mei, W. ~~(2019)~~: Tropical cyclone cold wake size and its applications to
611 power dissipation and ocean heat uptake estimates. ~~Geophysical Research~~ [Geophys. Res. Letters](#), 46(16), 10177-
612 10185, doi:10.1029/2019GL083783, [2019](#).

613 Zheng, Z. W., Ho, C. R., ~~&and~~ Kuo, N. J. ~~(2008)~~: Importance of pre-existing oceanic conditions to upper ocean
614 response induced by Super Typhoon Hai-Tang. ~~Geophysical Research~~ [Geophys. Res. Letters](#), 35(20),
615 doi:10.1029/2008GL035524, [2008](#).